JOURNAL OF GEOPHYSICAL RESEARCH, VOL. 103, NO. A9, PAGES 20,789-20,796, SEPTEMBER 1, 1998

Global observation of the ionospheric electronic response to solar events using ground and LEO GPS data

M. Hernández-Pajares, J. M. Juan, and J. Sanz

Group of Astronomy and Geomatics, Department of Applied Mathematics and Telematics, and Department of Applied Physics, Universitat Politècnica de Catalunya, Barcelona, Spain

J.G. Solé

Observatori de l'Ebre-CSIC-URL, Roquetes, Tarragona, Spain

Abstract. We present in this work the temporal evolution of the three–dimensional electron density at global scale during two ionospheric storms (October 18-19, 1995, and January 10, 1997) computed using only actual Global Positioning System data. The tomographic model is solved by means of a Kalman filtering with a filter updating time of 1 hour in a Sun-fixed reference frame, and with a resolution of 10x10 deg in latitude/local time and 100 km in height including also a protonospheric component (eight layers). The data set contains the data from the International GPS Service IGS (with more than 100 ground GPS stations worldwide distributed) and the GPS/MET low orbiting GPS receiver (both positive and negative elevation observations are used). This means for each storm 1,000,000 of delays, 400 occultations and 3000 unknowns per batch. The International Reference Ionosphere and data coming from the ionosonde of the Ebre observatory are used to show the reliability of the results.

1. Introduction

The capability of estimating the ionospheric electron density at global scale in any geomagnetic condition is important for the National Space Weather Program [*Szuszczewicz and Wilkinson*, 1997] and in general for the improvement in the knowledge of ionospheric storms [*Kamide et al.*, 1997].

Also, it has been demonstrated recently that the use of the electron density (tomographic) models at regional scale for navigation purposes provides better ionospheric corrections than the use of total electron content models which assumes that all the ionospheric free electrons are concentrated in a thin layer at fixed height [*Hansen et al.*, 1997).

In this context the purpose of this paper is to show that it is possible now to estimate at global scale the electron density of the ionosphere in high ionospheric variability conditions. This is done by means of a tomographic "only data driven" model solving with the Kalman filter the electronic densities of the ionosphere with the Global Positioning System (GPS) satellite dual frequency carrier phases, observed from the worldwide network of permanent receivers (International GPS Service, IGS [*Zumberge et al.*, 1994] and the low Earth orbiting (LEO) receiver GPS/MET [*Ware et al.*, 1995] (available at http://pocc.gpsmet.ucar.edu / over / sept-Summ_top.html). The data sets analyzed correspond to the magnetic cloud event of October 18-19, 1995, and to the January 6-11, 1997, coronal mass ejection (CME) event [*Peredo et al.*, 1997].

This paper is, in our opinion, the logical extension of the paper *Juan et al.* [1997] where a similar, but coarser, tomographic model (two layers: ionosphere and protonosphere) is solved during one ionospheric storm in November 1993 using only GPS ground data. In that work, it was demonstrated that the tomographic models improve also the total electron content and the instrumental bias estimates because in the nontomographic (one layer) models, these estimates capture part of the protonospheric electron content. Now, the limited vertical resolution of that work is improved with the use of the geometrically complementary LEO GPS receiver observations, as was predicted with simulations by *Hajj et al.* [1994] and *Howe et al.* [1998].

Paper number 98JA01272.
0148-0227/98/98JA-01272$09.00

2. The Model

2.1. Carrier Phase Preprocessing

The geodetic dual frequency GPS receivers usually provides, for each epoch and for each of the tracked satellites, typically 6 or 7 simultaneously, code phases (P_1 and P_2) and carrier phases ($\mathcal{L}_1$ and $\mathcal{L}_2$) in two L-band frequencies $f_1 \simeq 1575$ MHz and $f_2 \simeq 1227$ MHz, respectively. The carrier phases are very accurate with errors of 0.002 m or smaller [*Wells et al.*, 1986, page

9.14], being the result of the correlation between the incoming carrier with the receiver replica.

Physically, $\mathcal{L}_m$ $(m = 1,2)$ is the apparent range of the path described by the carrier of frequency f_m between the nominal transmission epoch $(\bar{t}^T)$ and the reception time $(\bar{t}_R)$ that is affected by an integer bias of wavelengths or "integer ambiguity" N_m:

$$\mathcal{L}_m = c(\bar{t}_R - \bar{t}^T) + \lambda_m N_m + \epsilon_m \quad m = 1,2$$

being c the speed of light, λ_m the wavelength, and $\sigma_{\epsilon_1} \simeq \sigma_{\epsilon_2} \simeq 0.002m$.

Then we can split the apparent range between receiver and transmitter in two terms:

1. R_0 as the frequency independent term, that is basically, in length units, the geometric delay due to the true range, affected by the difference in receiver-transmitter clocks, tropospheric delays and other minor contributions that are the same for both frequencies f_1 and f_2.

2. The δR_m that is the delay which depends on the frequency (f_m) and that can be written as

$$\delta R_m = -\frac{K}{f_m^2} \int_{\vec{r}^T(t^T)}^{\vec{r}_R(t_R)} N_e(\vec{r},t)\, ds + D_{m,R} + D_m^T$$

where $K = 40.28$ meters of delay $\cdot$ Hz^2 $\cdot$ m^2 [*Wells et al. 1986*, p. 9.05]; $\vec{r}^T$ and $\vec{r}_R$ are the positions of transmitter T and receiver R at true times t^T and t_R respectively; N_e is the free electron density along the ray path between T and R; $t \simeq t_R$; $D_{m,R}$ and D_m^T are respectively the instrumental biases for receiver R and transmitter T in the frequency f_m.

From here $(m = 1,2)$:

$$\mathcal{L}_m = R_0 + \delta R_m + \lambda_m N_m + \epsilon_m$$

$$\mathcal{L}_I = \kappa \int_{\vec{r}^T(t^T)}^{\vec{r}_R(t_R)} N_e(\vec{r},t)\, ds + D_R + D^T + \lambda_1 N_1 - \lambda_2 N_2 + \epsilon_I$$

where $\mathcal{L}_I \equiv \mathcal{L}_1 - \mathcal{L}_2$, $D_R = D_{1,R} - D_{2,R}$ and $D^T = D_1^T - D_2^T$ are the interfrequency biases for receiver R and transmitter T, $\kappa = K\left[1/f_2^2 - 1/f_1^2\right] \simeq 1.0506$ m delay $/10^{17}$ electrons/m^2 and $\sigma_{\epsilon_I} \simeq \sigma_{\epsilon_1} \simeq \sigma_{\epsilon_2} \simeq 0.002m$.

Finally, it remains yet the integer ambiguities term $\lambda_1 N_1 - \lambda_2 N_2$, that is constant within each arc of connected carrier phases (without "cycle–slips" [see *Blewitt*, 1990]). To cancel it, we consider differences between continuous phases for the same pair of transmitter T and receiver R differing in τ seconds. (Notice that in this way we avoid to align with the code to estimate this ambiguity term, and then we avoid the associated alignment error, specially important now with the Anti-Spoofing activated ($\simeq 0.3$ m).) This time must be sufficient to provide enough geometry variation of the ray to allow solving for the free electron densities in the tomographic problem, which we are going to describe in the next subsection, and small enough to suppose that the electron density does not change in a reference frame with the Sun fixed (for instance, for $\tau \simeq 720$ s the method works well).

Then, the final equation in the preprocessing stage is

$$\frac{\Delta\mathcal{L}_I}{\kappa} = \int_{\vec{r}^T(t^T+\tau)}^{\vec{r}_R(t_R+\tau)} N_e\, ds - \int_{\vec{r}^T(t^T)}^{\vec{r}_R(t_R)} N_e\, ds + \epsilon_I \quad (1)$$

being $\Delta\mathcal{L}_I \equiv \mathcal{L}_I(t+\tau) - \mathcal{L}_I(t)$ and $N_e \equiv N_e(\vec{r},t)$.

2.2. Tomographic Equation

We decompose the ionosphere in three–dimensional cells in the Sun fixed reference frame "local time/geodetic latitude / height" (see below). In these cells we assume that the electron density is constant (see Figure 1). Then the last equation (1), for each arc of continuous carrier phases between a transmitter T and receiver R becomes:

$$\frac{\Delta\mathcal{L}_I}{\kappa} = \sum_i \sum_j \sum_k (N_e)_{i,j,k} \left[\Delta s_{i,j,k}^{t+\tau} - \Delta s_{i,j,k}^{t}\right] + \epsilon_I \quad (2)$$

where i,j,k are the indices for each cell corresponding to local time, geodetic latitude and height; $(N_e)_{i,j,k}$ is

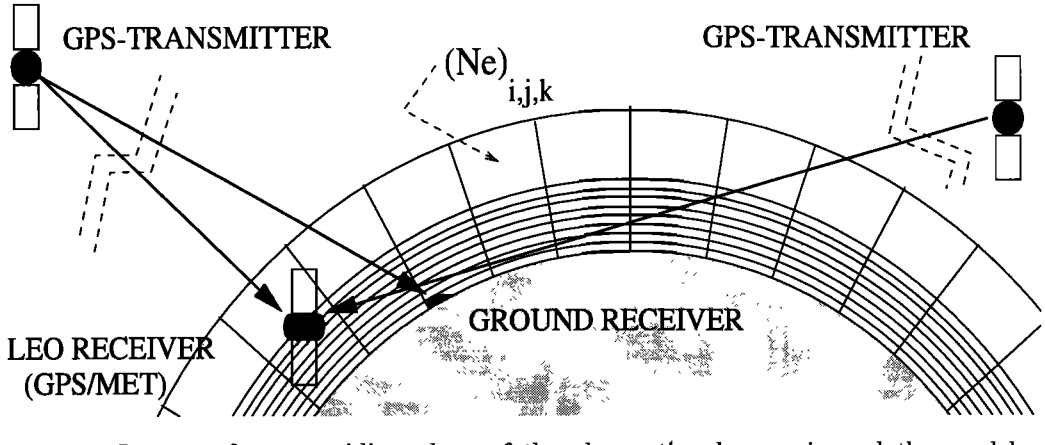

Figure 1. Layout of one meridian plane of the observational scenario and the model cells, representing one typical ground and LEO observation. The unknowns, electron densities, are also indicated.

the corresponding free electron density; and $\Delta s^t_{i,j,k}$ is the length of the ray path crossing the illuminated cells at time t ($\Delta s^t_{i,j,k} = 0$ for the "dark" cells).

In order to solve equation (2), and then to get the electronic density in an ionospheric storm scenario, we use the Kalman filter starting on with an initial solution obtained from longer batches in time during the previous quiet prestorm period.

The classical matricial solution of the Kalman filter, assuming a random walk process for the electron density in the mentioned Sun fixed reference frame, is

$$\overline{x}_{t_0+\Delta t} = \left[A^T C_y^{-1} A + (C_{\overline{x}_{t_0}} + \dot{Q}\cdot\Delta t)^{-1}\right]^{-1} \cdot \left[A^T C_y^{-1} y + (C_{\overline{x}_{t_0}} + \dot{Q}\cdot\Delta t)^{-1}\overline{x}_{t_0}\right] \quad (3)$$

where $\overline{x}_{t_0+\Delta t}$ is the vector of electron density estimates for the new batch at time $t_0 + \Delta t$; y is the vector containing the observations $[\mathcal{L}_I(t+\tau) - \mathcal{L}_I(t)]$ for the new batch at $t_0 + \Delta t$ with covariance matrix C_y; A is the matrix containing the corresponding length coefficients $(\Delta s^{t+\tau}_{i,j,k} - \Delta s^t_{i,j,k})$ for each given pair of rays separated by τ seconds in the same transmitter-receiver arc of continuous phase; $\overline{x}_{t_0}$ is the vector containing the estimates of the electron density $(N_e)_{i,j,k}$ for the batch at time t_0 with covariance $C_{\overline{x}_t}$. This covariance is increased, under the assumption of random walk process for the electron density, when we propagate the old solution to the batch at time $t_0 + \Delta t$, by an amount of $\dot{Q}\cdot\Delta t$.

3. Data Analysis

The vertical resolution, i.e., the number of layers, that can be successfully solved in the tomographic model is strongly limited when we only use ground data, because of the typical radial transmitter-receiver ray geometry [*Juan et al.*, 1997]. The limitation in the number of vertical layers can be overcome incorporating additional data from the low Earth orbiter (LEO) GPS receivers which rays present an orthogonal geometry with regard to the ground station rays [*Hajj et al.*, 1994] (see Figure 1).

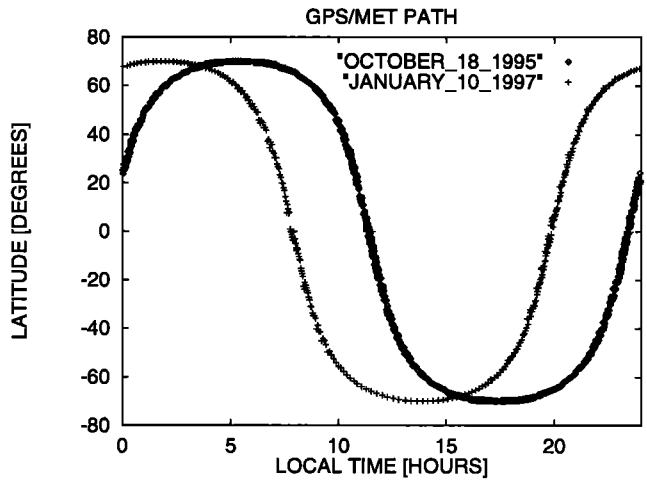

Figure 2. GPS/MET positions corresponding to the observation epochs of October 18, 1995, and January 10, 1995, tracing the region where we have the most information to reconstruct the vertical structure of the ionospheric electron density. The Sun is at 12 hours of local time.

The data sets considered correspond to October 18-19, 1995 (set A), and January 9-10, 1997 (set B). They consist on dual–frequency phases and codes measured in

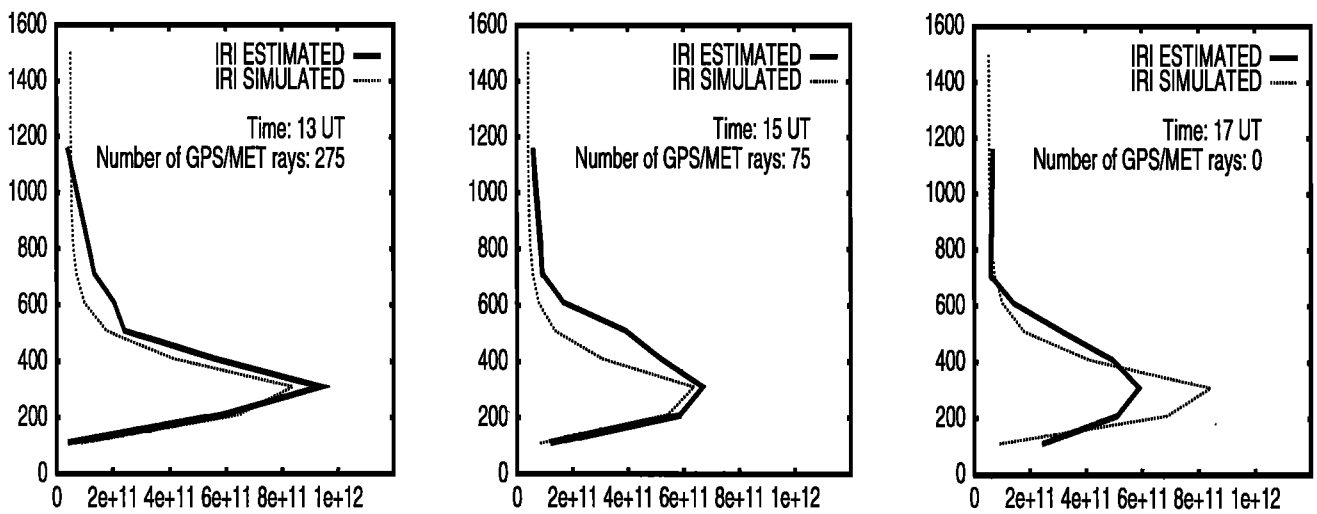

Figure 3. Comparison of the IRI retrieval for the ionospheric electron density (solid line) with the IRI values used in the simulations (dashed line) using the actual rays for October 18, 1995. The electron density is represented in the horizontal axis (ranging from 0 to 1.2×10^{12} electrons/m^3) and the vertical axis represents the height (from 0 to 1600 km). The three plots correspond to the same local time and latitude (10 hours and 10 deg respectively) at different times, (left) 1300, (middle) 1500, and (right) 1700 UT respectively, with different GPS/MET illumination (275, 75, and 0 rays respectively).

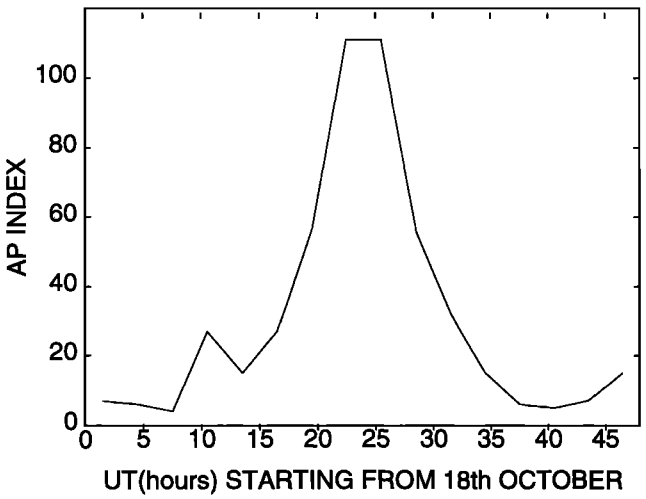

Figure 4. The *Ap* geomagnetic index is plotted for October 18 and 19, 1995 (time is expressed in hours from 0000 UT UT on October 18).

the IGS permanent GPS stations (115 in set A and 160 in set B) and in the GPS/MET receiver. The sampling interval used for data sets A and B was one observation per 2 min per visible satellite and per ground station (≃900,000 and 1,400,000 observations respectively) and one observation per 10 s for the GPS/MET (≃100,000 and 50,000 observations respectively including the data from ≃400 occultations each). The reason of the minor number of useful GPS/MET observations for the data set B were the higher number of cycle–slips found in the phase preprocessing. There is another a–priori disadvantage for set B in order to reconstruct the vertical distribution of the electron density: the GPS/MET observations are far from the Sun position (at 12 hours in the adopted reference frame), that is where the most electron content is expected (see Figure 2). For the tomographic study presented here we have selected the ionospheric region with latitudes ranging -40 to 80 deg because of the greater density of data.

In these particular data sets, as it was commented in the introduction, major ionospheric storms occurred as consequence of two solar events.

To estimate the electron density we use a model (equation (2)) with eight spherical layers with boundaries at heights of 60, 160, 260, 360, 460, 560, 660, 760 and 1560 km that have been chosen to provide a vertical resolution of 100 km under the GPS/MET orbit (seven layers) and estimating also the protonosphere (eighth layer, see Figure 1). Each shell has been divided in cells of 10×10 deg in local time and latitude.

To increase the spatial and temporal resolution of the model, we use the Kalman filter. We assume, as it was commented above, that the electron content variations between consecutive solutions are modeled as a random walk in a Sun-fixed reference frame. The solution for each batch is propagated to the next batch increasing

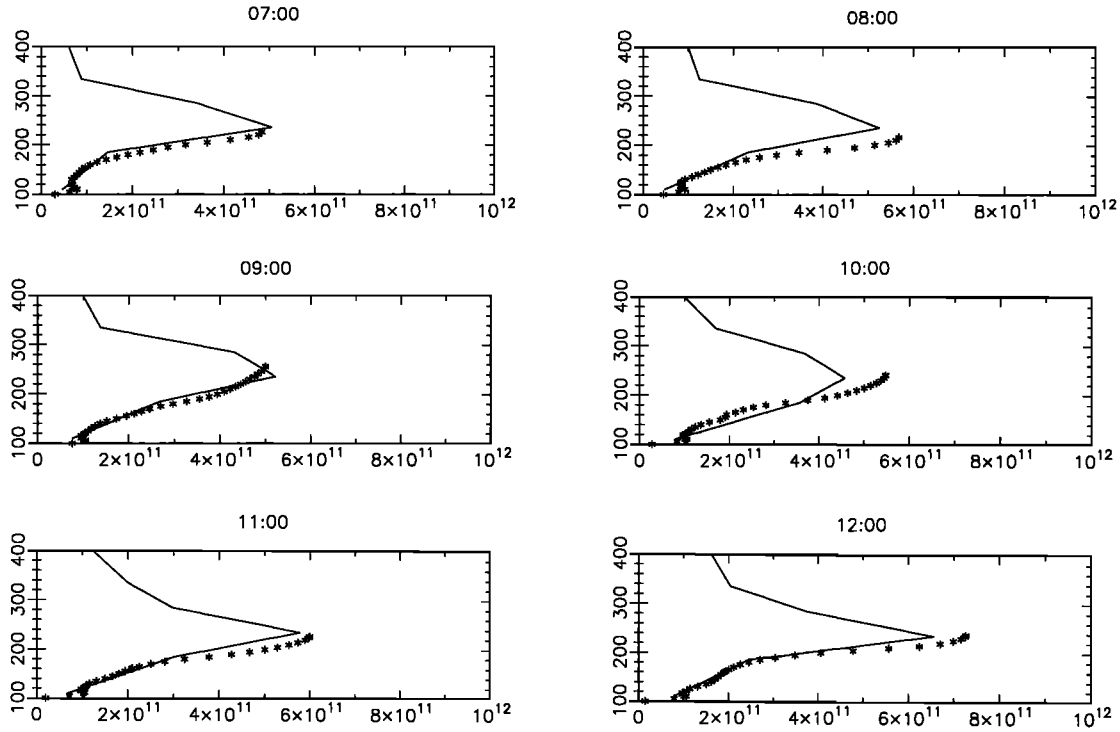

Figure 5. Comparison of the bottomside electron density profiles between Ebre observatory ionosonde and our results for October 18, 1995. The vertical axis contains the electron density ranging from 0 to 10^{12} electrons/m^3 and the vertical axis the height between 100 to 400 km. Each label indicates the UT that approximately corresponds with the local time at Ebre Observatory (0.5 deg of longitude).

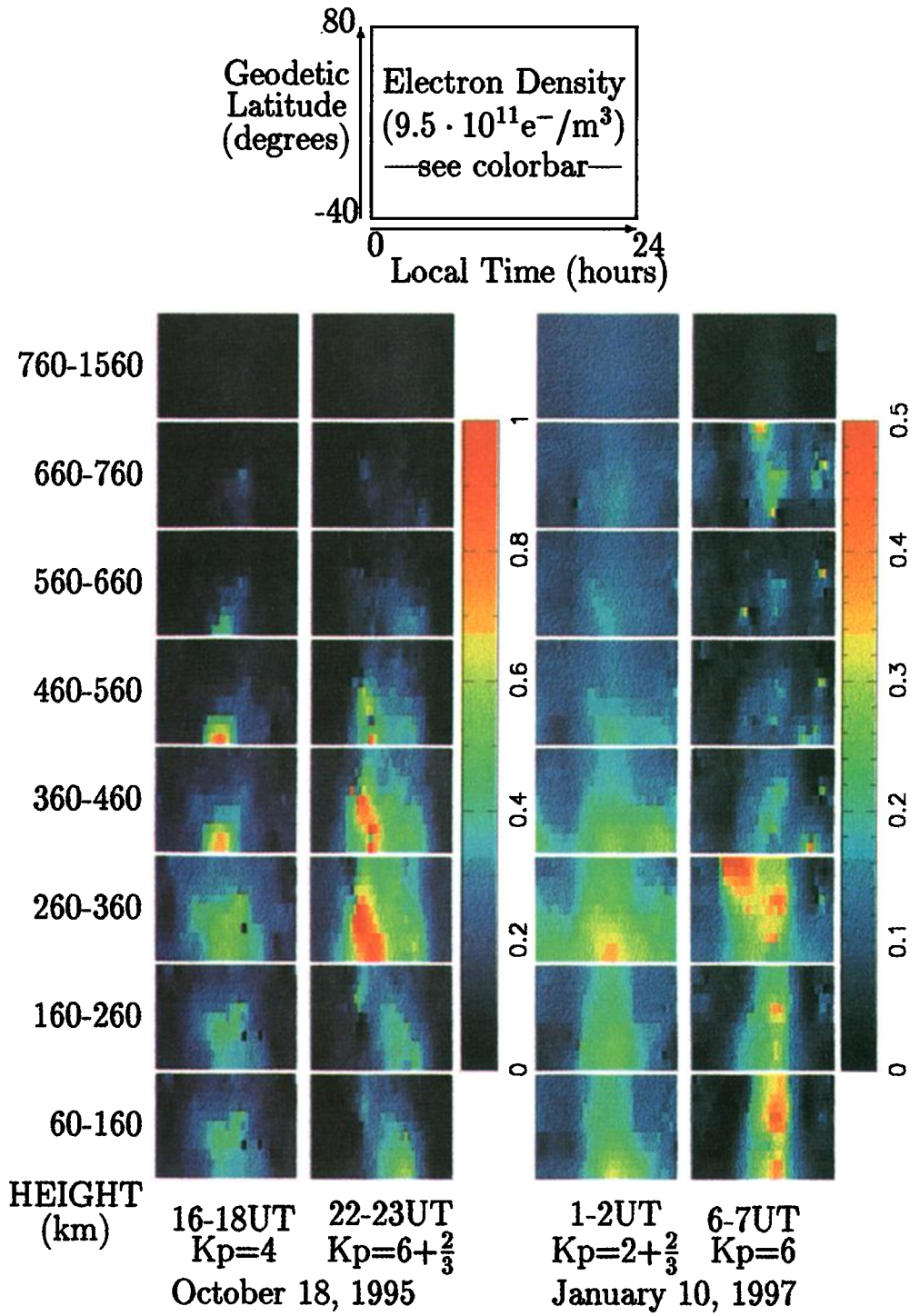

Plate 1. Sample of the results obtained for the ionospheric storms of October 18-19, 1995, (color scale between 0 and 10^{12} electrons/m^2 approximately) and January 9-10, 1997 (color scale between 0 and 5×10^{11} electrons/m^2). More details in the text.

their process noise covariance in such a way that each a priori value for the electronic density, considering the 8 cells in a given vertical direction, is approximately equivalent to one to ten observations in the inverse problem weighting. (We have typically about 2×10^4 new observations and 3×10^3 unknowns per batch.)

The integration time choosen for the batches in the Kalman filter must satisfy a compromise between to be large enough to allow the inclusion of new meaningful data with vertical information and to be short enough to get some evolution of the ionospheric storm when there are more variability. Then, it has been taken as of 1 hour

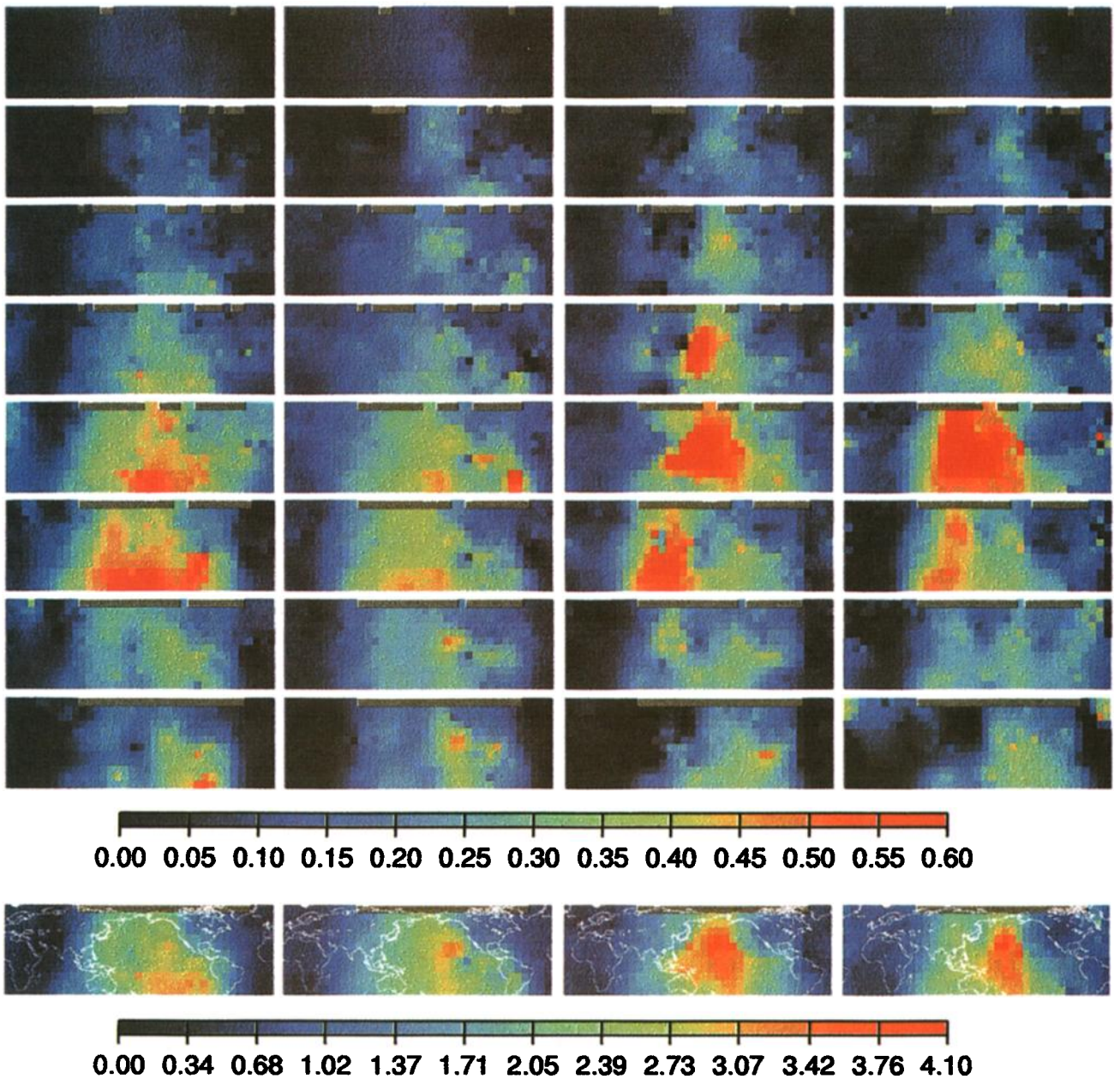

Plate 2. Electron density "movie" (top block of eight rows) and the corresponding total electron content (bottom row) along four consecutive time batches of one-hour: October 18, 2330 UT (first column) and October 19, 0030, 0130 and 0230UT (second, third, and fourth column) following the same representation than in Plate 1: The 8 layers in the top part of the figure are represented from top to bottom (1st row corresponds to the 8th layer and 8th row to 1st layer). The electron density runs from 0.00 to 0.60 in units of 9.5×10^{11}electrons/m^2 and the TEC from 0.00 to 4.10 in units of 10 TECU (10^{17} electrons/m^2). Each small plot represents the corresponding electron content estimate between -40 and 80 deg in latitude and 0 to 24 hours in local time.

for the storm study (January 10, 0000-2400 UT, October 18, 1200 UT-October 19, 1200 UT). Previously, and in order to get reliable a priori values to initialize the filter for the study of the storm, we have processed the pre–storm day, with higher time steps (8 and 4 hours being $\dot{Q}$ equal to $8{\cdot}\dot{Q}$"storm" and $4{\cdot}\dot{Q}$"storm" respectively in equation (3)). Only cells containing data are estimated, and this is the value propagated to the next batch in the Kalman filter process.

As was commented above, we perform all our computations in a Sun-fixed reference frame where the electronic distribution is more stationary. Then, the coordinate system chosen is "local time / geodetic latitude / height" being local time and geodetic latitude the spherical coordinates associated with the following reference system: the X-Y plane is the geodetic equator, the Z–axis points toward the North geodetic pole and the plane X-Z contains the Sun with "azimuthal" coordinate

of 180 deg (local time of 12 hours) and finally the Y-axis forms a positive oriented reference frame. With these choices the main part of the electronic distribution will appear in the center of the plots.

4. Results

We present the results at three levels: (1) assessment of the vertical reconstruction of the electron density, (2) electron density estimation with real data, and (3) validation.

4.1. Assessment of the Vertical Reconstruction of the Electron Density

Previously to the estimation with actual data and taking into account that the noise of the observations is very small and that the main problem is the reliability in the vertical reconstruction, we have analyzed the performance of the tomographic inversion: to test our model we have used the real rays (geometry) with the corresponding ionospheric delays following the electronic distribution of reference of the International Reference Ionosphere (IRI), [*Bilitza* 1990], instead of the observed one. (The error of 2 mm in $\mathcal{L}_I$ produce a typical error of $N_e \simeq 10^9$ electrons/m^3 very small compared with the typical electronic densities of 10^{10}-10^{12} electrons/m^3.)

In Figure 3 we can see the comparison between the vertical profiles of the reference electron density simulated by IRI and the corresponding one to the electron density reconstruction with our model.

This is done for data set A, and similar results are obtained with the data set B. Notice that the tomography works well in areas illuminated by the GPS/MET observations and still typically maintains the maximum density height in most of the areas without GPS/MET observations but with a certain "smoothing" of the electron density profile.

As it was commented above, in the data set B the GPS/MET observations are mainly concentrated in the night hemisphere far to the Sun, and this is the reason of a worst reconstruction in the day hemisphere, reaching an overestimating of $\simeq 20\%$ of the layer 1 close to the Sun, at 12 hours local time.

4.2. Electron Density Estimation With Real Data

As a summary of our results with the actual data, in Plate 1 we show the global electron density estimates of the ionosphere during two Kalman batches for each storm, for one relatively quiet and for one geomagnetic active period (the *Kp* indices have been provided by NOAA, see, for example, Geomagnetic and solar data (October 1995). The two first columns correspond to the October 18, 1995, and the last two columns to the January 10, 1997. Each column run the eight layers and each plot-box represents in the color scale the estimated electron density in local time/latitude coordinates as it is also shown in Plate 1. These results, using only experimental data, show how much can the three-dimensional electron distribution increase along ionospheric storms.

Also, we present a sample of the "movie" of images directly representing the electron density estimates each hour during the maximum geomagnetic activity (see Figure 4): between October 18, 2330 UT and October 19, 0230 UT the October 18-19, 1995 (Plate 2). The total electron content, as far as the continents are also represented at bottom in Plate 2. In this way we present an example of the short-term patterns of the ionospheric response detected at global scale using exclusively GPS data.

5. Validation

The comparison of the GPS global estimate with other systems is presented in Figure 5 for October 18, 1995, with bottomside electron density profiles obtained with the ionosonde of the Ebre Observatory at Roquetes, Spain (0.5 deg of longitude and 40.8 deg of latitude). A reasonable agreement is found between these results still with the 0700 and 0800 UT profiles performed at $\simeq$ 50 deg of the simultaneous GPS/MET observations (see Figure 2 taking into account that the UT approximately corresponds with the local time at Ebre Observatory which is placed approximately at the Greenwich meridian and that the latitude of Ebre observatory is approximately 40 deg).

More comparisons with other ionosonde profiles at different latitudes as far as with the Millstone Hill observatory radar estimates will be treated in future works.

Acknowledgments. We acknowledge the support of IGS and UCAR for providing the ground and GPS/MET receiver data. We are thankful to D. Bilitza for providing the IRI model and to JPL/CALTECH for using GIPSY in the ground data preprocessing. Plate 2 was produced with the software package GMT, of *Wessel and Smith* [1995]. This work has been partially supported by the Spanish CICYT project TIC97-0993-C02-01.

The Editor thanks the referees for their assistance in evaluating this paper.

References

Bilitza, D., International Reference Ionosphere 1990. URSI / COSPAR, NSSDC/WDC-A-R&S 90-22, 1990.

Blewitt, G., An automatic editing algorithm for GPS data, *Geophys. Res. Lett.*, *17*, 199-202, 1990.

Hajj, G.A., R. Ibañez-Meier, E.R. Kursinski, and L.J. Romans, Imaging the ionosphere with the Global Positioning System, *Imag. Syst. Technol.*, *5*, 174-184, 1994.

Hansen, A.J., T. Walker, and P. Enge, Ionospheric correction using tomography, paper presented at GPS'97, Inst. of Nav., Kansas City, Mo., Sept. 1997.

Howe, B. M., K. Runciman, and J. A. Secan, Tomography of the ionosphere: Four-dimensional simulations, *Radio Sci.*, *33*, 109-128, 1998.

Juan, J.M., A. Rius, M. Hernández-Pajares, and J. Sanz, A two-layer model of the ionosphere using Global Positioning System data, *Geophys. Res. Lett.*, *24*, 393-396, 1997.

Kamide, Y., R.L. McPherron, W.D. Gonzalez, D.C. Hamilton, H.S. Hudson, J.A. Joselyn, S.W. Kahler, L.R. Lyons, H. Lundstedt, and E. Szuszczewicz, *Magnetic Storms: Current Understanding and Outstanding Questions*, *Geophys. Monogr. Ser.*, vol. 98, edited by B.T. Tsurutani, W.T. Gonzalez, Y. Kamide, and J.K. Arballo, pp. 1-19, AGU, Washington, D.C., 1997.

Peredo, M., N. Fox, and B. Thompson, Scientists track solar event all the way to Earth, *Eos Trans. AGU*, 78(43), **477, 483, 1997.**

Szuszczewicz, E.P., and P.J. Wilkinson, On the accuracy of ionospheric electron density measurements by complementary "in situ" and remote sensing techniques: Langmuir probes and ionosondes, *Eos Trans. AGU*, *78*(46), Fall Meet. Suppl., F512, 1997.

Ware, R.H., M.L. Exner, B.M. Herman, Y-H. Kuo, T.K. Meehan, and C. Rocken, GPS/MET, preliminary report, operated by The University Corporation for Atmospheric Research and sponsored by The National Science Foundation, The Federal Aviation Administration and The National Oceanic and Atmospheric Administration, July 1995.

Wells, D., et al., *Guide to GPS Positioning*, Can. GPS Assoc., Fredericton N.B., Canada, 1986.

Wessel, P. and W.H.F. Smith, New version of the generic mapping tools released, *Eos Trans. AGU*, *76*, 326, 1995.

Zumberge, J., R. Neilan, G. Beutler, and W. Gurtner, The International GPS Service for Geodynamics-Benefits to Users, paper presented at GPS-94 Meeting, Inst. of Nav., Salt Lake City, Utah, Sept. 20-23, 1994.

M. Hernández-Pajares, J. M. Juan, and J. Sanz, Group of Astronomy and Geomatics, Department of Applied Mathematics and Telematics, Campus Nord. mod. C3, Universitat Politècnica de Catalunya, Jordi Girona 1 i 3, 08034 Barcelona, Spain. (e-mail: manuel@mat.upc.es)

J. G. Solé, Observatori de L'Ebre-CSIC-URL, 43620 Roquetes, Tarragona, Spain. (e-mail: ebre.gsole@readysoft.es)

(Received March 17, 1998; accepted March 23, 1998.)